Decorrelation of L-Band and C-Band Interferometry Over Vegetated Areas in California

Meng Wei and David T. Sandwell

***Abstract*—Temporal decorrelation is one of the main limitations for recovering interseismic deformation along the San Andreas Fault system using interferometric synthetic aperture radar. To assess the improved correlation properties of L-band with respect to C-band, we analyzed L-band Advanced Land Observation Satellite (ALOS) interferograms with a range of temporal and spatial baselines over three vegetated areas in California and compared them with corresponding C-band European Remote Sensing Satellite (ERS) interferograms. Over the highly vegetated Northern California forests in the Coast Range area, ALOS remains remarkably well correlated over a 2-year period, whereas an ERS interferogram with a similar temporal and spatial baseline lost correlation. In Central California near Parkfield, we found a similar pattern in decorrelation behavior, which enabled the recovery of a fault creep and a local uplifting signal at L-band that was not apparent at C-band. In the Imperial Valley in Southern California, both ALOS and ERS have low correlation over farmlands. ALOS has lower correlation over some sandy surfaces than ERS, probably due to low signal-to-noise ratio. In general, L-band interferograms with similar seasonal acquisitions have higher correlation than those with dissimilar season. For both L- and C-band, correlation over vegetated areas decreases with time for intervals less than 1 year and then remains relatively constant at longer time intervals. The decorrelation time for L-band is more than 2 years in the forest in California whereas that for C-band is less than 6 months. Overall, these results suggest that L-band interferograms will reveal near-fault interseismic deformation once sufficient data become available.**

***Index Terms*—Correlation, crustal deformation, interferometry, synthetic aperture radar (SAR).**

I. Introduction

INTERFEROMETRIC synthetic aperture radar (InSAR) has become an important tool for measuring slow surface deformation associated with natural hazards such as earthquakes and volcanoes [1]–[3]. One of the main limitations of the InSAR technique is temporal decorrelation due to surface change, particularly in vegetated areas, because the low correlation prevents the recovery of the phase measurement. The Advanced Land Observation Satellite (ALOS) launched by the Japanese Aerospace Exploration Agency (JAXA) in January 2006 uses a longer wavelength L-band 236 mm, compared to the C-band radars 56 mm (European Remote Sensing Satellite (ERS), Radarsat, and Envisat), which should enable coherent phase recovery over much longer time intervals in vegetated areas [4]–[6], such as the creeping section of the San Andreas Fault (SAF). Key parameters of ALOS and ERS satellites are listed in Table I. Although previous theoretical and limited experimental studies suggest this advantage of the longer wavelength synthetic aperture radar (SAR) over vegetated areas, here, we perform a more extensive and quantitative analysis using ALOS and ERS data over a variety of surfaces, temporal baselines, and spatial baselines. Our main objective is to provide a quantitative measure of temporal decorrelation at L- and C-band. Our results provide insights and suggestions for future SAR missions such

TABLE I
COMPARISON OF SATELLITES

	ERS	ALOS
Wavelength	56 mm	236 mm
Altitude	790 km	700 km
Look angle*	23 degrees	34.3 degrees
Bandwidth	15.55 MHz	FBS: 28 MHz FBD: 14 MHz
Critical Baseline	1.1 km	FBS: 13 km FBD: 6.5 km

*Other look angles are available for ALOS, but 34.3 degrees is the main one.

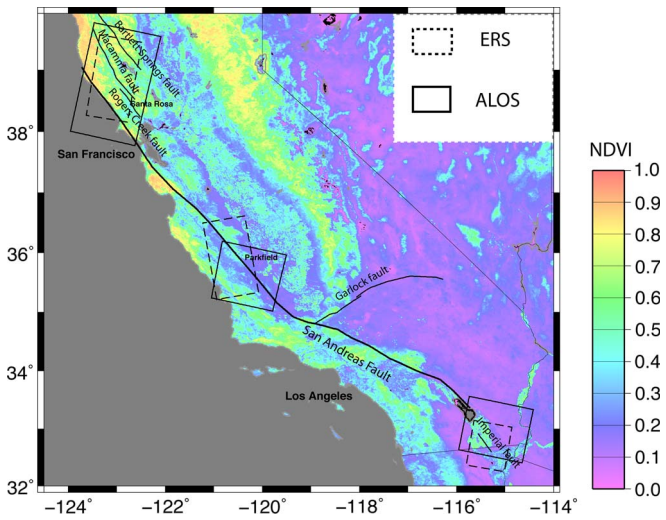

Fig. 1. Three research areas in California: 1) the Coast Ranges in Northern California; 2) the creeping section of the San Andreas Fault near Parkfield in Central California; and 3) the Imperial Valley in Southern California. The color background indicates NDVI acquired by MODIS satellite in October 2006. The purple background means no or little vegetation, whereas the green means high vegetation. The solid lines show the main fault traces. The solid and dashed boxes show the coverage of InSAR images used in this work.

Manuscript received October 20, 2009; revised December 2, 2009 and January 15, 2010. This work was supported in part by the National Science Foundation Geophysics Program under Contract EAR 0811772 and the National Aeronautics and Space Administration EarthScope Program—The InSAR and Geodetic Imaging Component under Contract NNX09AD12G.

The authors are with the Scripps Institution of Oceanography, University of California at San Diego, La Jolla, CA 92093-0225 USA (e-mail: mwei@ucsd.edu; dsandwell@ucsd.edu).

Color versions of one or more of the figures in this paper are available online at http://ieeexplore.ieee.org.

Digital Object Identifier 10.1109/TGRS.2010.2043442

TABLE II
INTERFEROGRAMS USED FOR DIRECT CORRELATION COMPARISON

	Interferograms	1st date	2nd date	Interval (days)	Baseline (m)	Correlation				
Coast Ranges in Northern California						Mountain 1	Mountain 2	Urban		
ALOS T549F2830	4357_15093 (FBS-FBS)	11/18/06	11/23/08	736	252	0.35	0.27	0.35		
ERS T113F2817/2835	e1_22646_e2_13995	11/13/95	12/23/97	770	110	0.14	0.13	0.23		
Creeping Section of the SAF in Central California						Mountain 1	Mountain 2	Urban		
ALOS T220F700	5969_16705 (FBS-FBS)	3/9/07	3/14/09	735	905	0.25	0.28	0.34		
ERS T256F2889	e2_05621_e2_17144	5/17/96	7/31/98	804	68	0.14	0.25	0.24		
Imperial Valley in Southern California						Farmland 1	Farmland 2	Urban	Sand 1	Sand 2
ALOS T532F2960	4167_14903 (FBS-FBS)	11/5/06	11/10/08	736	17	0.16	0.13	0.53	0.30	0.17
ERS T84F2943	e2_03445_e2_12463	12/17/95	9/7/97	629	55	0.15	0.14	0.28	0.34	0.46

as the U.S. satellite DESDynl, Japanese satellite ALOS2, and German satellite TanDEM-L.

Correlation, sometimes called coherence, is a measure of the similarity of the phase of two SAR images. Theoretically, correlation ranges between 0 and 1, where 0 denotes no correlation, and 1 corresponds to perfect correlation. In practice, a number of pixels are weighed to estimate the correlation [7]. In our case, correlation is measured from approximately 45 independent pixels, equivalent to 3 looks in range and 15 looks in azimuth direction [2], and the detectable range of correlation is slightly different from theory with the minimum being 0.12 and the maximum being 0.96 in our calculation. A correlation of 0.5 marks a signal-to-noise ratio (SNR) of 1 in linear scale [8]. As shown in previous works [5] and in our work, there is a critical range of correlation between 0.15 and 0.20 that determines whether an interferogram is usable. When the correlation is larger than 0.20, phase information can be retrieved and becomes better when correlation increases; when correlation is between 0.15 and 0.20, it is possible but hard to retrieve some phase information; and when the correlation is below 0.15, no phase information can be retrieved. Generally, high correlation (> 0.20) is expected in areas where the surface condition does not change much with time, such as in urban areas, and low correlation is expected where vegetation is present. Techniques such as permanent scatterers can be used to extract phase information in areas where a few local stable reflection points are imbedded in an area of generally low correlation [9]. Correlation is also important for topography measurements [6]. In this paper, we analyzed L-band ALOS interferograms over three vegetated areas in California and compared them with corresponding C-band ERS interferograms. Our results are consistent with previous suggestions that L-band has higher correlation over vegetated areas than C-band and correlation depends on the type of surface.

II. THEORY

Most InSAR satellites are designed as repeat-pass, which means a single radar acquires images of the same area at two different times, usually with a repeat time of 10–50 days. The detailed theory and mathematical derivation of correlation can be found in several previous studies [1], [6]. We present the relevant equations here. Assume that pixels of the complex radar images for first and second acquisition are

$$\begin{aligned} s_1 &= c + n_1 \\ s_2 &= c + n_2 \end{aligned} \tag{1}$$

where c is correlated part of the signal, and n_1 and n_2 are the uncorrelated noise caused by baseline, temporal, thermal, rotation, and other unknown factors.

One measure of the correlation between two images is

$$\gamma = \frac{\left|\langle s_1 s_2^* \rangle\right|}{\sqrt{\langle s_1 s_1^* \rangle \langle s_2 s_2^* \rangle}} \tag{2}$$

where s^* is the complex conjugate of s, and $\langle \cdot \rangle$ denotes ensemble average. When the two radar images are exactly the same, correlation equals one, and when they are completely different, the correlation approaches zero. The total correlation mainly consists of the following three parts: 1) thermal γ_{thermal}; 2) spatial γ_{spatial}; and 3) temporal γ_{temporal} decorrelation [4], [6], [10]. We have

$$\gamma = \gamma_{\text{thermal}} \gamma_{\text{spatial}} \gamma_{\text{temporal}} \tag{3}$$

where γ is the total correlation. The thermal decorrelation is related to the SNR of the radar signal as

$$\gamma_{\text{thermal}} = \frac{1}{1 + \text{SNR}^{-1}}. \tag{4}$$

In most cases, the SNR for ERS and ALOS is high enough to ignore this effect [10]. Exceptions include special cases such as L-band over a sandy surface where the SNR is significantly lower [1]. The spatial decorrelation is caused by the nonzero perpendicular baseline between the reference and repeat images [6], [11]–[13]. There are two effects of spatial decorrelation, namely: 1) volumetric decorrelation and 2) surface decorrelation. For area with high penetration, such as pine forests [14] and ice [15], volume decorrelation dominates. However in our case, no significant volume decorrelation is observed, thus, we only consider spatial decorrelation related to surface scatterers. There are two ways to estimate the spatial decorrelation. One way is by using a range spectral filter [16], and the other way is by using the following model [6]. If the satellite has a

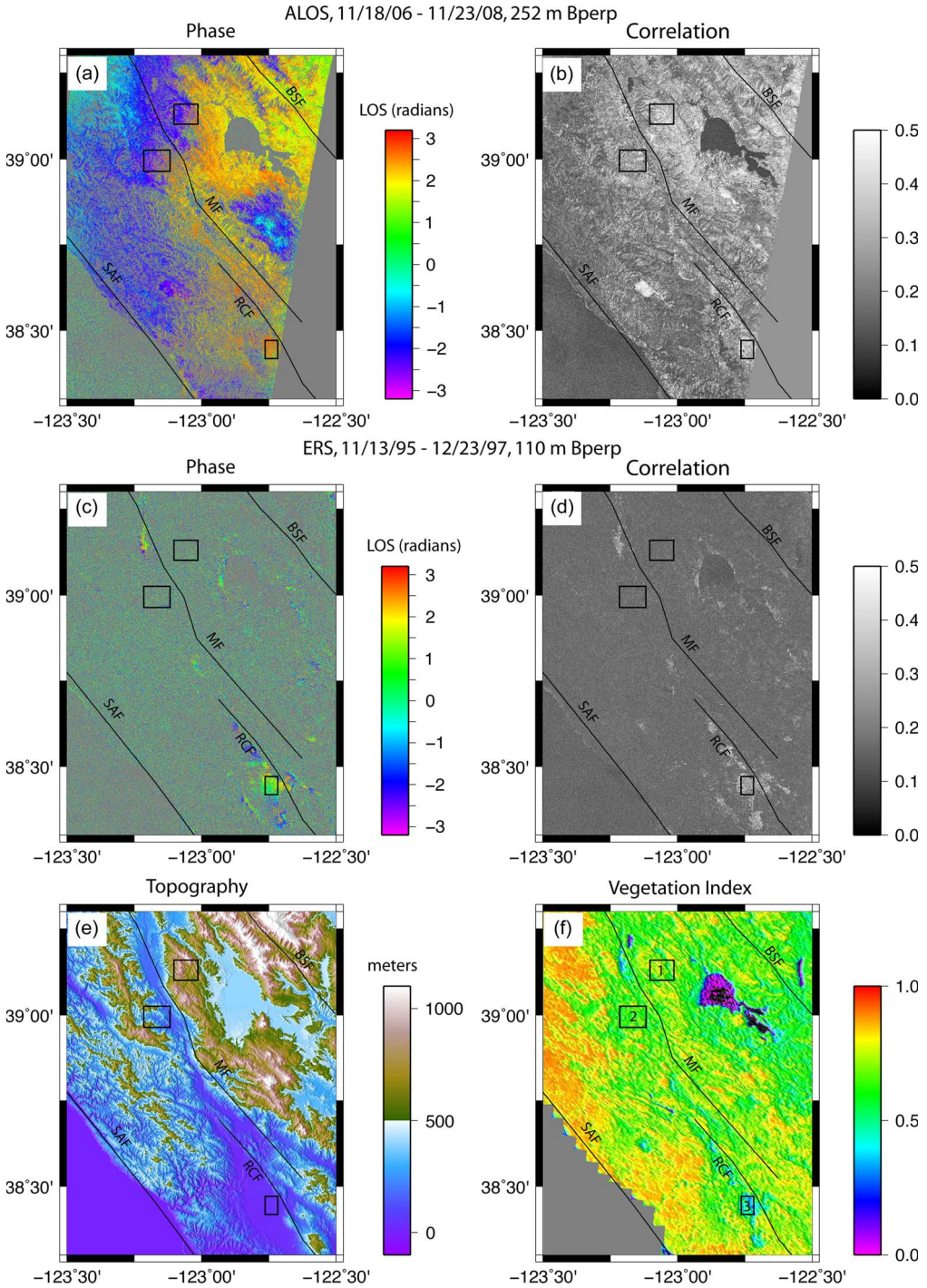

Fig. 2. Comparison between ERS and ALOS interferograms in the Coast Range area in Northern California. The details of the interferograms are shown in Table II. The solid lines are the major faults in this area. Fault names are abbreviated as follows: SAF, San Andreas Fault; MF, Maacama Fault; RCF, Rogers Creek Fault; and BSF, Bartlett Springs Fault. The boxes are the areas from which correlation is extracted in Table II and Fig. 5. The box number in (f) indicates the corresponding areas in Fig. 5: (1) vegetated mountain 1; (2) vegetated mountain 2; and (3) urban areas. The phase images are masked based on the correlation (< 0.15 is masked out). White in (b) and (d) means high correlation, whereas black means low correlation. The red and green in (f) means high vegetation, whereas purple means low vegetation.

perpendicular baseline of B, the spatial correlation between the two radar images is

$$\gamma_{\text{spatial}} = 1 - \frac{2|B|R_y \cos^2(\theta - \alpha)}{\lambda \rho} \tag{5}$$

where R_y is the range resolution, θ is the incidence angle, α is the local surface slope in range direction, λ is the wavelength, and ρ is the distance between the satellite sensor and the target on the surface. This equation is used to isolate the temporal decorrelation from the measured decorrelation in the following analysis. When correcting spatial decorrelation using this equation, we need to make sure that no bandpass filtering is done during the processing. The temporal decorrelation is caused by surface changes between the two acquisitions. Generally, temporal decorrelation increases with the amount of vegetation cover because the scatterers on the plants change with time [4].

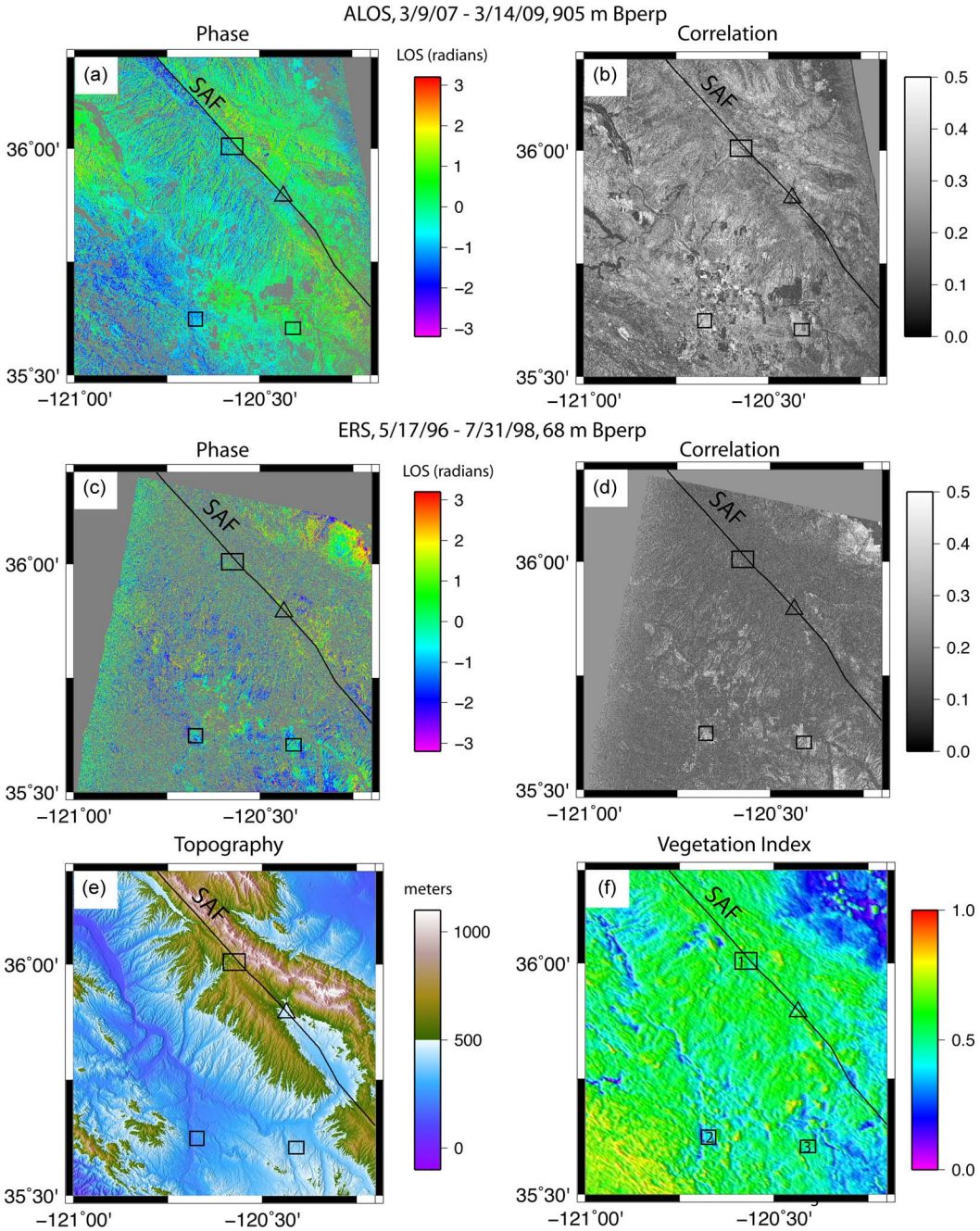

Fig. 3. Comparison between ERS and ALOS interferograms near Parkfield in Central California. The details of the interferograms are shown in Table II. The solid line is the fault trace of the San Andreas Fault in this area. The triangle is the city of Parkfield. The boxes are the areas from which correlation is extracted in Table II and Fig. 6. The box number in (f) indicates the corresponding areas in Fig. 6: (1) vegetated mountain 1; (2) vegetated mountain 2; and (3) urban areas. The phase images are masked based on the correlation (< 0.15 is masked out).

With sufficiently high SNR and low volumetric decorrelation, temporal decorrelation can be isolated after removing the spatial decorrelation.

III. Data and Method

To compare the correlation of interferograms of ERS and ALOS, we processed interferograms over the following three vegetated areas in California (Fig. 1): 1) the Coast Ranges in Northern California; 2) the creeping section of the SAF near Parkfield in Central California; and 3) the Imperial Valley in Southern California. The ERS data were provided by the European Space Agency and obtained through the Western North America Interferometric Synthetic Aperture Radar Consortium archive. ALOS data were provided by JAXA and obtained through the Alaska Satellite Facility as well as the ALOS User Interface Gateway.

Since ALOS has limited acquisition in California and the baseline has been drifting by more than 6 km after launch, we found only one interferogram in each area that was suitable for direct comparison (see Table II) (the baseline has been controlled to within a 3-km tube since early 2008). To focus on temporal decorrelation, we search for long time intervals (> 10 months) and short baselines (< 200 m for ERS; < 2 km

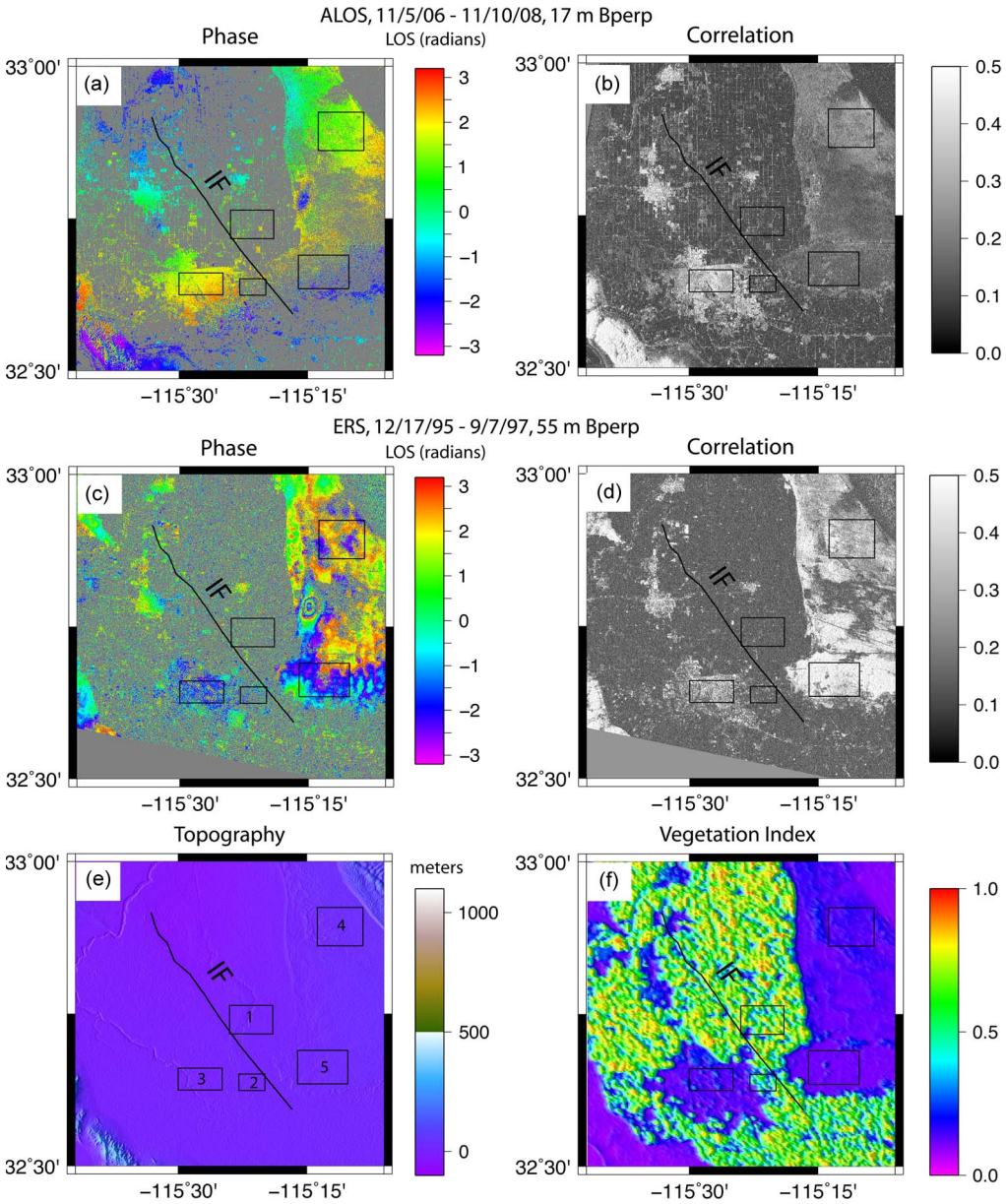

Fig. 4. Comparison between ERS and ALOS interferograms in Imperial Valley in Southern California. The details of the interferograms are shown in Table II. The solid line is the fault trace of the Imperial Fault. The boxes in (e) are the areas from which correlation is extracted in Fig. 7. The phase changing area in the middle right on both phase images is due to subsidence caused by underground water extraction. The box number in (f) indicates the corresponding areas in Fig. 7: (1) farmland 1; (2) farmland 2; (3) urban areas; (4) sand 1; and (5) sand 2. The phase images are masked based on the correlation (< 0.15 is masked out).

for ALOS). Since the number of ALOS acquisitions is much smaller than the number of ERS acquisitions, we first selected the best ALOS interferogram and then found an ERS interferogram with corresponding baseline, time interval, and season(s). Even within a single interferogram, the correlation can be highly spatially variable, depending on the type of surface and degree of vegetation. Therefore, we selected several corresponding subareas within the overlapping ALOS and ERS frames corresponding to no vegetation, light vegetation, and heavy vegetation. The sizes of the patches were small enough to cover one particular kind of surface but are large enough to provide meaningful statistics; the chosen patch size (length/width of a rectangle) varies from 3 to 7 km, depending on the surface condition.

The normalized difference vegetation index (NDVI) provides an overview of the vegetation along the SAF system (Fig. 1). The NDVI data were collected by Moderate Resolution Imaging Spectroradiometer (MODIS) satellite and obtained through National Aeronautics and Space Administration Warehouse Inventory Search Tool website. The NDVI indicates the concentrations of green leaf vegetation quantitatively. Although many possible perturbing factors exist, the NDVI can be used to identify the surface vegetation. Comparing the NDVI with the correlation in Figs. 2–4, we observed that when the NDVI is less than 0.3, both ERS and ALOS interferograms have high correlation.

All interferograms were processed following the standard procedure of InSAR processing using SIOSAR software [17].

TABLE III
INTERFEROGRAMS USED IN THIS WORK

	Interferograms	1st date	2nd date	Interval (days)	Baseline (m)	Correlation				
Coast Ranges in Northern California						Mountain 1	Mountain 2	Urban		
ALOS T549F2830	4357_15093 (FBS-FBS)	11/18/06	11/23/08	736	252	0.35	0.27	0.35		
	8383_9054 (FBS-FBS)	8/21/07	10/6/07	46	479	0.67	0.54	0.41		
	8383_9725 (FBS-FBS)	8/21/07	11/21/07	92	727	0.49	0.33	0.25		
	8383_10396 (FBS-FBS)	8/21/07	1/6/08	138	1132	0.16	0.18	0.13		
	9054_9725 (FBS-FBS)	10/6/07	11/21/07	46	248	0.64	0.44	0.42		
	9054_10396 (FBS-FBS)	10/6/07	1/6/08	92	654	0.17	0.18	0.27		
	9725_10396 (FBS-FBS)	11/21/07	1/6/08	46	405	0.22	0.28	0.40		
ERS T113F2817/2835	e1_21644_e2_06981	9/4/95	8/20/96	351	82	0.17	0.17	0.32		
	e1_21644_e2_09486	9/4/95	2/11/97	525	108	0.14	0.13	0.24		
	e1_22646_e2_13995	11/13/95	12/23/97	770	110	0.14	0.13	0.23		
	e2_06981_e2_09486	8/20/96	2/11/97	174	190	0.15	0.14	0.23		
	e2_06981_e2_17001	8/20/96	7/21/98	699	180	0.14	0.14	0.25		
	e2_09486_e2_17001	2/11/97	7/21/98	525	10	0.14	0.16	0.14		
Creeping Section of the SAF in Central California						Mountain 1	Mountain 2	Urban		
ALOS T220F700	7311_8653 (FBD-FBD)	6/9/07	9/9/07	92	540	0.57	0.40	0.48		
	7311_12008 (FBD-FBD)	6/9/07	4/26/08	322	2662	0.15	0.19	0.23		
	7311_16705(FBD-FBS)	6/9/07	3/14/09	643	906	0.18	0.20	0.25		
	7311_18047(FBD-FBD)	6/9/07	6/14/09	735	873	0.23	0.26	0.33		
	5969_7311 (FBS-FBD)	3/9/07	6/9/07	92	2	0.39	0.29	0.33		
	5969_8653 (FBS-FBD)	3/9/07	9/9/07	184	557	0.34	0.27	0.29		
	5969_12008 (FBS-FBD)	3/9/07	4/26/08	414	2579	0.15	0.20	0.23		
	5969_16705 (FBS-FBS)	3/9/07	3/14/09	735	905	0.25	0.28	0.34		
	5969_18047 (FBS-FBD)	3/9/07	6/14/09	827	872	0.17	0.19	0.23		
	8653_12008 (FBD-FBD)	9/9/07	4/26/08	230	2049	0.18	0.23	0.28		
ERS T256F2889	e2_05621_e2_10130	5/17/96	3/28/97	314	111	0.16	0.29	0.26		
	e2_05621_e2_17144	5/17/96	7/31/98	804	68	0.14	0.25	0.24		
	e2_05621_e2_17645	5/17/96	9/4/98	839	11	0.15	0.18	0.25		
	e2_08627_e2_09629	12/13/96	2/21/97	70	123	0.17	0.26	0.26		
	e2_08627_e2_12635	12/13/96	9/19/97	280	44	0.16	0.24	0.24		
	e2_09629_e2_11132	2/21/97	6/6/97	105	7	0.19	0.38	0.30		
	e2_09629_e2_11633	2/21/97	7/11/97	140	76	0.17	0.32	0.27		
	e2_10130_e2_12134	3/28/97	8/15/97	140	82	0.18	0.35	0.27		
	e2_11132_e2_11633	6/6/97	7/11/97	35	69	0.46	0.71	0.45		
Imperial Valley in Southern California						Farmland 1	Farmland 2	Urban	Sand 1	Sand 2
ALOS T532F2960	4167_5509 (FBS-FBD)	11/5/06	2/5/07	92	1614	0.21	0.14	0.37	0.29	0.17
	5509_9535 (FBD-FBS)	2/5/07	11/8/07	276	1048	0.16	0.12	0.19	0.27	0.09
	5509_10877 (FBD-FBS)	2/5/07	2/8/08	368	1994	0.14	0.10	0.25	0.16	0.13
	5509_15574 (FBD-WS1)	2/5/07	12/26/08	782	1044	0.09	0.08	0.42	0.12	0.20
	5509_16245 (FBD-FBS)	2/5/07	2/10/09	735	803	0.12	0.11	0.35	0.17	0.14
	9535_10877 (FBS-FBS)	11/8/07	2/8/08	92	892.9	0.29	0.17	0.33	0.29	0.16
	14903_16245 (FBS-FBS)	11/10/08	2/10/09	92	740	0.30	0.18	0.28	0.36	0.12
	4167_9535 (FBS-FBS)	11/5/06	11/8/07	368	2703	0.10	0.09	0.52	0.12	0.18
	4167_10877 (FBS-FBS)	11/5/06	2/8/08	460	3649	0.12	0.09	0.53	0.19	0.17
	4167_14903 (FBS-FBS)	11/5/06	11/10/08	736	17	0.16	0.13	0.53	0.30	0.17
	4167_16245 (FBS-FBS)	11/5/06	2/10/09	827	747	0.13	0.11	0.54	0.22	0.21
ERS T84F2943	e2_03445_e2_12463	12/17/95	9/7/97	629	55	0.15	0.14	0.28	0.34	0.46
	e2_10960_e2_11461	5/25/97	6/29/97	35	226	0.29	0.17	0.41	0.49	0.50
	e2_10960_e2_11962	5/25/97	8/3/97	70	32	0.28	0.17	0.47	0.57	0.61
	e2_11461_e2_14467	6/29/97	1/25/98	210	3	0.18	0.14	0.37	0.41	0.47
	e2_12463_e2_13966	9/7/97	12/21/97	105	223	0.18	0.14	0.31	0.37	0.40

Shuttle Radar Topography Mission (SRTM) data [18] were used to remove the topographic effect from the single-look complex interferograms prior to ensemble averaging. All interferograms were ensemble averaged using a Gaussian filter with a 0.5 gain at 100 m wavelength before computing the phase and correlation, which is equivalent to 3 looks in range and 15 looks in azimuth in more popular InSAR processors such as ROI-PAC [2]. Based on this filter width, we find the minimum detectable correlation is 0.12 based on ocean data where the correlation should be zero.

IV. RESULTS

A. Comparison of Interferograms With Similar Temporal and Spatial Baselines

The correlation results for the three areas are shown in Figs. 2–4 along with the local NVDI and topography. Although the value of correlation can theoretically range between 0 (uncorrelated) to 1 (perfectly correlated), our analysis is focused on the range of 0.15–0.20. In all three areas, ALOS remains correlated over longer time intervals than ERS does over vegetated surfaces. In urban areas, ALOS tends to have higher correlation. In farmlands, neither ALOS nor ERS has high correlation because of the cultivation activity. However, the details are different for each area.

1) Coast Ranges in Northern California: Major faults in this area include the SAF, the Maacama Fault, the Rodgers Creek Fault, and the Bartlett Spring Fault. This area is studied less extensively than the other two areas because it is far from major cities and is in a mainly mountainous area. Limited previous studies used global positioning satellite (GPS) and creepmeter measurements. Because of this sparse geodetic coverage, the contribution to our understanding of these fault systems from ALOS could be significant. Over 90% of the area is covered with trees, except for the farmlands and urban areas near the city of Santa Rosa. To compare the correlation

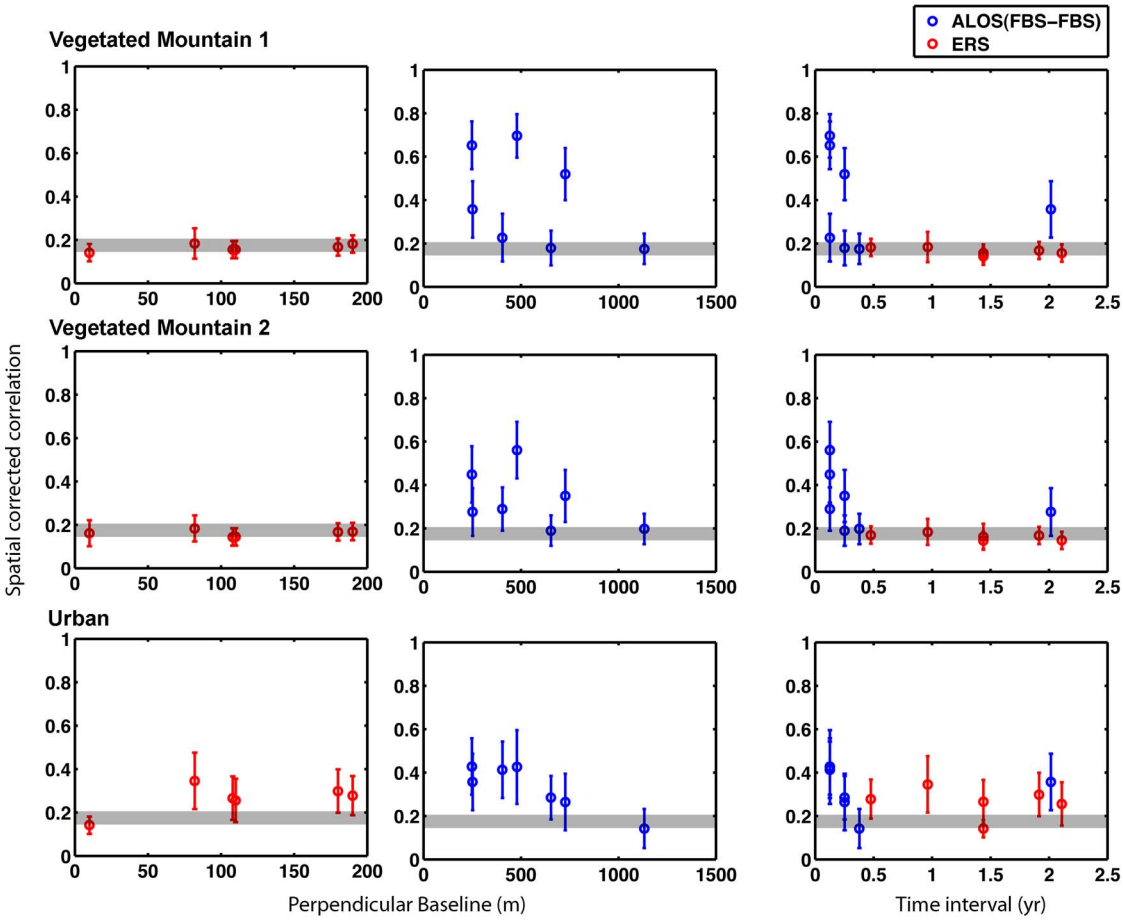

Fig. 5. Spatially corrected correlation changes with baseline and time on three types of surface in the Coast Range area in Northern California (Table III). All ALOS data are FBS–FBS mode. The horizontal gray line marks the range 0.15–0.2 correlation. Data above the gray line are well correlated, and almost all the phase information can be used. Data in the gray line are partially correlated, and it is possible to retrieve some phase information. Data below the gray line are decorrelated, and no phase information can be retrieved. Each row shows data over the same area. Each column shows data with same kind but in different areas.

of ALOS and ERS, two interferograms are selected (Table II). The ALOS interferogram has a 2-year November-to-November time interval and a perpendicular baseline of 252 m. The ERS interferogram has a 2-year November-to-December time interval and a perpendicular baseline of 110 m. As Fig. 2 shows, the ALOS interferogram has high correlation (> 0.27) over most of the land area, whereas the ERS interferogram has generally low correlation (< 0.13), except in the urban area near Santa Rosa. The values of correlation for the three subareas are provided in Table II. The ALOS interferogram has better correlation not only in the vegetated areas but also in the urban areas.

2) Creeping Section of the SAF Near Parkfield in Central California: This area is particularly scientifically interesting because of its regular pattern of magnitude 5–6 earthquakes and a transition from creeping in the northern section to locked fault in the southern section [19], [20]. Previous studies show that InSAR can measure the continuous slip distribution and magnitude of fault motion along the SAF [17]. However, because of the temporal decorrelation, the previous C-band interferograms cannot provide a long-time (> 2 years) measurement of deformation in this area [21]. The two interferograms that we chose for direct comparison are given as follows: 1) an ALOS interferogram with a 2-year March-to-March time interval and a perpendicular baseline of 905 m and 2) an ERS interferogram with a 2-year May-to-July time interval and a perpendicular baseline of 68 m (Table II). As shown in Fig. 3, ERS has generally low correlation over the vegetated mountains, whereas ALOS is generally well correlated. The detailed comparison of correlation over different surfaces is provided in Table II. One important feature of the ALOS phase is that there is a correlation between residual phase and topography. The large-scale (> 5 km) residual is probably due to atmospheric error, whereas the small-scale (< 1 km) residual is probably due to either digital elevation model error or small misregistration between topography and interferogram.

3) Imperial Valley in Southern California: The Imperial Valley between the Colorado River and the Salton Sea contains some of the most seismically active faults along the SAF system including those with well-documented instances of surface rupture and triggered slip [17]. Much of the Imperial Fault is covered by farmlands, which makes it difficult to measure interseismic deformation using InSAR, although clear signs of slip such as cracks on roads are observed [22]. The interferograms selected for direct comparison are listed as follows: 1) an ALOS interferogram with a 2-year November-to-November time interval and a perpendicular baseline of 17 m and 2) an ERS interferogram with a 2-year December-to-September time

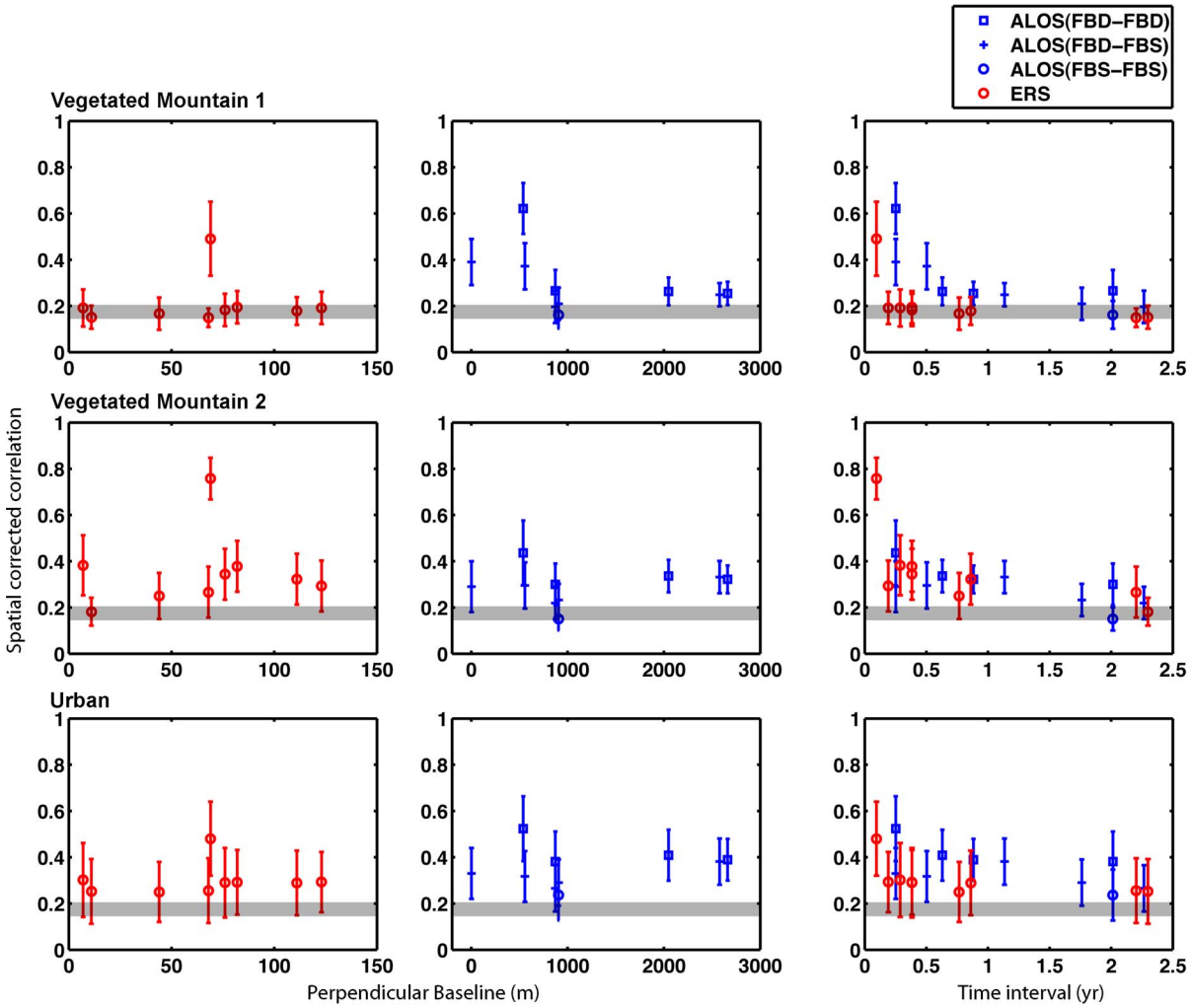

Fig. 6. Spatially corrected correlation changes with baseline and time on three types of surface near Parkfield in Central California (Table III). ALOS data are either FBS–FBS mode or mixed mode, e.g., FBS–FBD or FBD–FBS. The horizontal gray line marks the range 0.15–0.2 correlation.

interval and a perpendicular baseline of 55 m (Table II). As shown in Fig. 4, both ALOS and ERS have generally low correlation over the farmlands. A detailed comparison of correlation over a variety of surfaces is provided in Table II. ALOS has higher correlation over urban areas, whereas ERS has higher correlation over the sandy surface to the east of the valley, probably due to low SNR for L-band over sandy surface [1]. Although ALOS is decorrelated over the irrigated farmlands, the correlation remains high on some roads between farmlands; this makes it possible to recover some deformation signal across the Imperial Fault. We also note that the correlation over farmlands in the U.S. (northern side of the U.S.–Mexico border) is generally higher than the correlation in Mexico (southern side). This could be due to differences in cultivation methods of these different countries.

B. *Temporal Decorrelation*

To focus on the seasonal effect of the correlation, we processed data acquired during various seasons and analyzed the result for both ALOS and ERS (Table III). As expected, the interferograms with similar seasons for both acquisitions have better correlation compared with those with dissimilar seasons. However, we do not have enough data spanning all the seasons to identify a preferred season.

To focus on the temporal decorrelation and its relationship to surface type, we processed interferograms and chose four surface types, including vegetated mountain, farmland, urban area, and sandy area (Table III). For each interferogram, we extracted the mean and standard deviation of correlation in small sub areas (3–7 km in length/width). Since spatial decorrelation is related to the slope of the surface, we selected these areas to be as flat as possible, except in mountainous areas. We included the local slope effect when we estimated the spatial decorrelation. With sufficiently high SNR and low volumetric decorrelation, we isolated temporal decorrelation after removing the spatial decorrelation (Figs. 5–7). To check whether volumetric decorrelation exists, we plotted the spatial corrected correlation versus perpendicular baseline. We also plotted the temporal correlation versus time interval. The boundary between partial and poor correlation, i.e., 0.15–0.20, is highlighted in Figs. 5–7 as gray lines.

For the ERS cases, the spatially corrected correlation does not change much with spatial baseline over all the surface

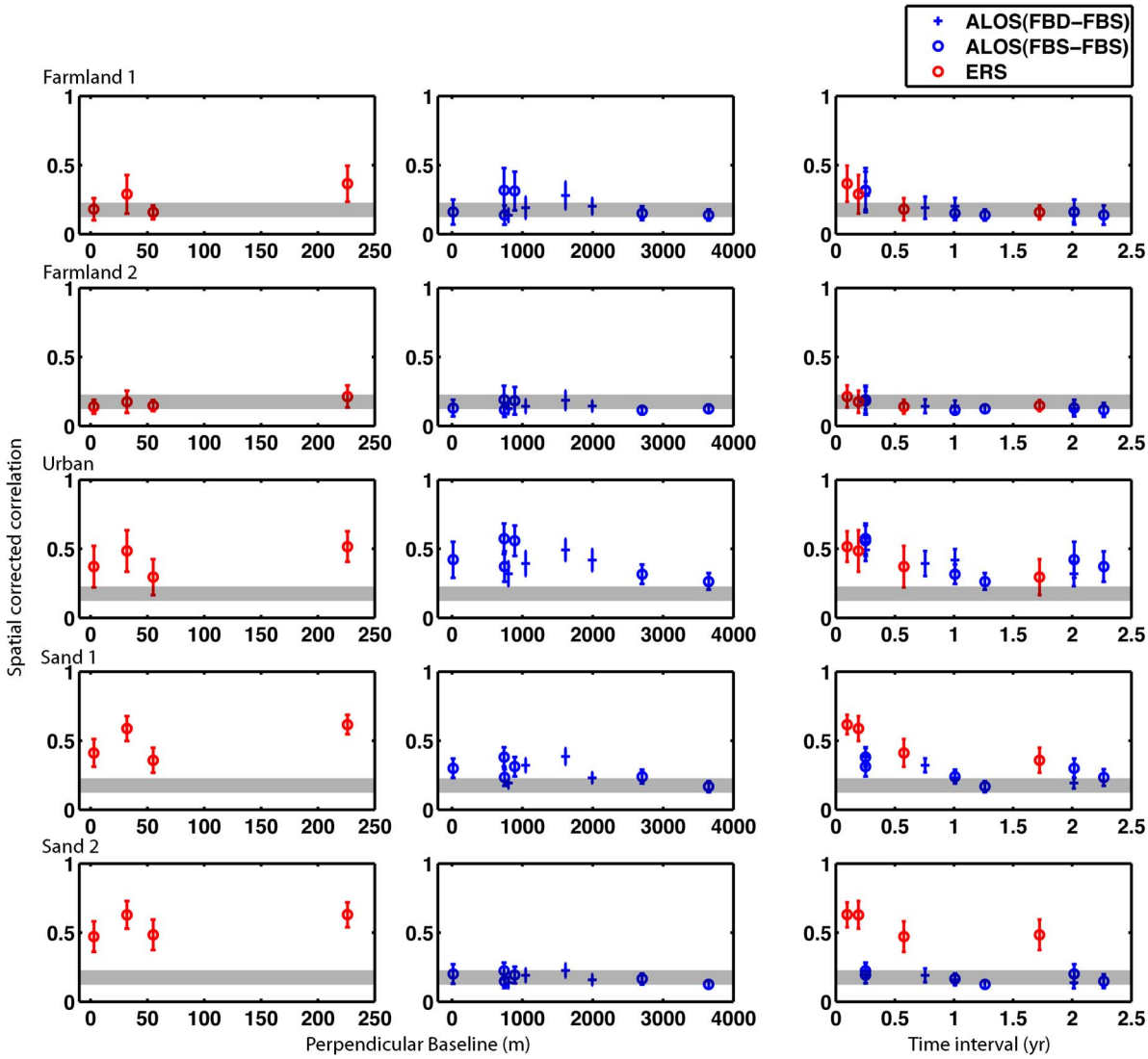

Fig. 7. Spatially corrected correlation changes with baseline and time on five types of surface in the Imperial Valley in Southern California (Table III). ALOS data are either FBS–FBS mode or mixed mode, e.g., FBS–FBD or FBD–FBS. The horizontal gray line marks the range 0.15–0.2 correlation.

types in the three areas, which means that spatial decorrelation correction works well and confirms our assumption of low volume decorrelation for C-band. A high correlation anomaly for ERS exists in the creeping section (see left panel in Fig. 6) might simply be due to the short time interval (35 days). The correlation over vegetation decreases with time when the time interval is less than 6 months in both Central California and Southern California (see Figs. 6 and 7) and becomes uniform for intervals greater than 1 year. In Northern California (see Fig. 5), all samples over forests are below the critical line and the minimum time interval of the sample is 6 months. In the urban area, the correlation stays above the critical line and shows that the buildings are good stable scatterers.

For the ALOS cases, no volumetric decorrelation is observed. Although Fig. 5 shows decreasing trends of correlation with increasing baseline in the Northern California case, this might be due to seasonal effect more than volumetric. All the pairs with low correlation cover the winter season. In Northern California and Central California, correlation over vegetation decreases with time when time interval is less than 1 year. For time intervals greater than 1 year, the correlation remains constant and sometimes increases with time interval. In Northern California, one interferogram with a 2-year interval has higher correlation than several interferograms with only a 2–3-month interval over vegetation. This illustrates the scattered nature of the temporal effects perhaps due to rainfall and soil moisture. The ability of ALOS to remain correlated above the 0.2 threshold for multiyear intervals is critical for measuring slow interseismic deformation, which ranges from several millimeters per year to several centimeters per year. Indeed, as more short-baseline ALOS interferograms become available over the next few years, we expect that ALOS will become the primary tool for resolving the near-fault interseismic strain rate that is not resolved by the relatively sparse (~10 km) GPS measurements.

One feature of ALOS is that it is operated at two different range resolutions (i.e., 1/radar bandwidth). The fine-beam single polarization (FBS-HH, 28-MHz bandwidth) has two times better range resolution than ERS, and the fine-beam dual polarization (FBD-HH and HV, 14 MHz) has the same range

resolution as ERS. ALOS interferograms can be made between either same modes or mixed modes, although conversion from FBD to FBS is required. In some cases, the correlation of FBS–FBS interferograms was slightly higher than that of mixed-mode interferograms, i.e., FBD–FBS. For example, in Fig. 7, FBS–FBS interferograms with time interval longer than 6 months have significantly higher correlation than the mixed-mode interferograms, particularly in the urban area. However, there is not much difference for interferograms with FBD–FBD compared to mixed-mode interferograms in Central California. Therefore, high correlation for FBS–FBS is probably due to the fact that FBS has higher resolution than FBD.

As Fig. 7 shows, ALOS has lower correlation than ERS over some sandy areas. This has been observed before by Rosen *et al.* [1]. This is likely due to the low SNR for L-band over sandy areas. We checked the amplitude image of the data, which confirmed this idea. In addition, both ALOS and ERS lost coherence over farmlands in the Imperial Valley within 6 months, which shows that L-band has no advantage over C-band over farmlands. However, we notice that L-band stays well correlated on the roads between farmlands, whereas C-band lost coherence. With a sufficient data set, it is possible to extract deformation data across the fault using the phase recovered on the roads in ALOS.

V. Conclusion

We compared one ALOS interferogram with the corresponding ERS interferogram with similar temporal and spatial baselines in each area. 1) In the highly vegetated Northern California forests of the Coast Range area, ALOS remained remarkably well correlated over a 2-year winter-to-winter interferogram (~ 0.27), whereas an ERS interferogram with similar temporal and spatial baselines was below the threshold correlation (< 0.13). 2) In Central California near Parkfield, we found a similar pattern. Four ALOS interferograms with a 2-year temporal baseline all had adequate correlation (0.16–0.25) over vegetated mountain areas, whereas the ERS interferogram had inadequate correlation (0.13–0.16). This improvement in correlation at L-band revealed creep and a local uplifting along the SAF that was not apparent at C-band (Fig. 3). 3) In the Imperial Valley in Southern California, ALOS had higher correlation in both the urban area (0.4 versus 0.3) and lightly irrigated area (0.18 versus 0.16). However, it had lower correlation over some sandy surfaces (0.2 versus 0.4).

Analysis of temporal decorrelation shows that correlation decreases with time, particularly for intervals between 0 and 1 year and then remains relatively constant after 1 year. The decorrelation time over forest for ALOS is more than 2 years, whereas for ERS, it is less than 6 months. Both ALOS and ERS decorrelated rapidly over farmlands. Seasonal effects are important. We also found in some cases, for example, in the desert and urban areas in the Imperial Valley (Fig. 7), that the correlation of FBS–FBS interferograms was slightly better than that of mixed-mode interferograms (i.e., FBD–FBS) and FBD–FBD, probably due to higher resolution of FBS.

Overall, these results demonstrate that ALOS remains correlated much longer than ERS over forest areas but not farmlands in California. To date, the primary limitation for using ALOS for recovering interseismic strain along the SAF is that there are too few acquisitions along the descending passes, which have better geometry for measuring strike–slip motion. Nevertheless, the archive of ALOS images from ascending passes is growing rapidly, and they will be important for constraining the vertical motions along the fault system. We look forward to the more systematic L-band observations from ALOS-2 (2014 launch), DESDynI (2016-2020 launch), and German satellite TanDEM-L (TBD).

Acknowledgment

The authors would like to thank Y. Fialko, D. Kilb, and K. Luttrell for the internal review of this paper, F. Meyer and an anonymous reviewer for the insightful suggestions about this paper, and H. Zebker, P. Rosen, E. Fielding, R. Burgmann, K. Fiegl, M. Simons, and R. Mellors for the discussions of this paper.

References

[1] P. A. Rosen, S. Hensley, I. R. Joughin, F. K. Li, S. N. Madsen, E. Rodriguez, and R. M. Goldstein, "Synthetic aperture radar interferometry," *Proc. IEEE*, vol. 88, no. 3, pp. 333–382, Mar. 2000.

[2] R. Burgmann, P. A. Rosen, and E. J. Fielding, "Synthetic aperture radar interferometry to measure Earth's surface topography and its deformation," *Annu. Rev. Earth Planetary Sci.*, vol. 28, pp. 169–209, 2000.

[3] D. Massonnet and K. L. Feigl, "Radar interferometry and its application to changes in the Earth's surface," *Rev. Geophys.*, vol. 36, no. 4, pp. 441–500, 1998.

[4] P. A. Rosen, S. Hensley, H. A. Zebker, F. H. Webb, and E. J. Fielding, "Surface deformation and coherence measurements of Kilauea volcano, Hawaii, from SIR-C radar interferometry," *J. Geophys. Res.—Planets*, vol. 101, no. E10, pp. 23 109–23 125, 1996.

[5] D. T. Sandwell, D. Myer, R. Mellors, M. Shimada, B. Brooks, and J. Foster, "Accuracy and resolution of ALOS interferometry: Vector deformation maps of the father's day intrusion at Kilauea," *IEEE Trans. Geosci. Remote Sens.*, vol. 46, no. 11, pp. 3524–3534, Nov. 2008.

[6] H. A. Zebker and J. Villasenor, "Decorrelation in interferometric radar echoes," *IEEE Trans. Geosci. Remote Sens.*, vol. 30, no. 5, pp. 950–959, Sep. 1992.

[7] R. Touzi, A. Lopes, J. Bruniquel, and P. W. Vachon, "Coherence estimation for SAR imagery," *IEEE Trans. Geosci. Remote Sens.*, vol. 37, no. 1, pp. 135–149, Jan. 1999.

[8] J. S. Bendat and A. G. Piersol, *Random Data: Analysis and Measurement Procedures*, 3rd ed. New York: Wiley, 2000.

[9] I. Ferretti, C. Prati, and F. Rocca, "Permanent scatterers in SAR interferometry," *IEEE Trans. Geosci. Remote Sens.*, vol. 39, no. 1, pp. 8–20, Jan. 2001.

[10] W. Hoen and H. A. Zebker, "Penetration depths inferred from interferometric volume decorrelation observed over the Greenland ice sheet," *IEEE Trans. Geosci. Remote Sens.*, vol. 38, no. 6, pp. 2571–2583, Nov. 2000.

[11] F. Li and R. M. Goldstein, "Studies of multi-baseline spaceborne interferometric synthetic aperture radars," *IEEE Trans. Geosci. Remote Sens.*, vol. 28, no. 1, pp. 88–97, Jan. 1990.

[12] E. Rodriguez and J. Martin, "Theory and design of interferometric synthetic aperture radars," *Proc. Inst. Elect. Eng.—F*, vol. 139, no. 2, pp. 147–159, Apr. 1992.

[13] I. Hajnsek, F. Kugler, S. K. Lee, and K. P. Papathanassiou, "Tropical-forest-parameter estimation by means of Pol-InSAR: The INDREX-II campaign," *IEEE Trans. Geosci. Remote Sens.*, vol. 47, no. 2, pp. 481–493, Feb. 2009.

[14] F. Garestier, P. C. Dubois-Fernandez, and I. Champion, "Forest height inversion using high-resolution P-band Pol-InSAR data," *IEEE Trans. Geosci. Remote Sens.*, vol. 46, no. 11, pp. 3544–3559, Nov. 2008.

[15] K. Langley, S. Hamran, K. A. Hogda, R. Storvold, O. Brandt, J. O. Hagen, and J. Kohler, "Use of C-band ground penetrating radar to determine backscatter sources within glaciers," *IEEE Trans. Geosci. Remote Sens.*, vol. 45, no. 5, pp. 1236–1246, May 2007.

[16] F. Gatelli, A. M. Guamieri, F. Parizzi, P. Pasquali, C. Prati, and F. Rocca, "The wavenumber shift in SAR interferometry," *IEEE Trans. Geosci. Remote Sens.*, vol. 32, no. 4, pp. 855–865, Jul. 1994.

[17] M. Wei, D. Sandwell, and Y. Fialko, "A silent Mw 4.7 slip event of October 2006 on the Superstition Hills fault, Southern California," *J. Geophys. Res.*, vol. 114, no. B7, p. B07 402, Jul. 2009, DOI:10.1029/2008JB006135.

[18] T. G. Farr, P. A. Rosen, E. Caro, R. Crippen, R. Duren, S. Hensley, M. Kobrick, M. Paller, E. Rodriguez, L. Roth, D. Seal, S. Shaffer, J. Shimada, J. Umland, M. Werner, M. Oskin, D. Burbank, and D. Alsdorf, "The shuttle radar topography mission," *Rev. Geophys.*, vol. 45, no. 2, p. RG2 004, May 2007.

[19] S. J. Titus, C. DeMets, and B. Tikoff, "Thirty-five-year creep rates for the creeping segment of the San Andreas fault and the effects of the 2004 Parkfield earthquake: Constraints from alignment arrays, continuous global positioning system, and creepmeters," *Bull. Seismol. Soc. Amer.*, vol. 96, no. 4B, pp. S250–S268, Sep. 2006.

[20] I. A. Johanson and R. Bürgmann, "Creep and quakes on the northern transition zone of the San Andreas fault from GPS and InSAR data," *Geophys. Res. Lett*, vol. 32, no. 14, p. L14 306, 2005.

[21] P. Rosen, C. Werner, E. Fielding, S. Hensley, S. Bukley, and P. Vincent, "Aseismic creep along the San Andreas Fault northwest of Parkfield, CA measured by radar interferometry," *Geophys. Res. Lett.*, vol. 25, no. 6, pp. 825–828, 1998.

[22] S. N. Lyons, Y. Bock, and D. T. Sandwell, "Creep along the imperial fault, Southern California, from GPS measurements," *J. Geophys. Res.*, vol. 107, no. B10, p. 2249, 2002, DOI:10.1029/2001JB000763.

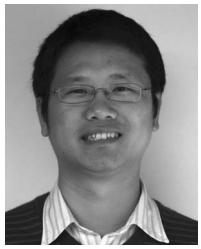

Meng Wei received the B.S. degree in geophysics from Peking University, Beijing, China, in 2004. He is currently working toward the Ph.D. degree in geophysics at the Scripps Institution of Oceanography, University of California at San Diego, La Jolla, with research focused on the observation and modeling of shallow fault creep in California.

His research interests include InSAR, GPS, fault zone processes, and crustal-deformation modeling.

David T. Sandwell received the B.S. degree in physics from the University of Connecticut, Storrs, in 1975 and the Ph.D. degree in geophysics and space physics from University of California, Los Angeles, in 1981.

Since 1994, he has been a Professor of geophysics at the Scripps Institution of Oceanography, University of California at San Diego, La Jolla. He is a member of the ALOS PALSAR Calibration and Validation Team. His main research interests include satellite geodesy, crustal deformation, and marine geophysics.

Dr. Sandwell is the President of the Geodesy Section of the American Geophysical Union.